Received: 20 May 2020 | Revised: 27 September 2020 | Accepted: 30 September 2020

DOI: 10.1002/app.50231

ARTICLE

Journal of Applied Polymer Science WILEY

Nanomechanical study of polycarbonate/boehmite nanoparticles/epoxy ternary composite and their interphases

Natalia Cano Murillo[1,3] | Media Ghasem Zadeh Khorasani[1] | Dorothee Silbernagl[1] | Marc Benjamin Hahn[1,2] | Vasile-Dan Hodoroaba[1] | Heinz Sturm[1,3]

[1]Division 6.6 Physical and Chemical Analysis of Polymers, Bundesanstalt für Materialforschung und–prüfung (BAM), Berlin, Germany

[2]School of Physics, Universidad Nacional de Colombia sede Medellín, Medellín, Colombia

[3]Department of Mechanical Engineering and Transport Systems, Technical University of Berlin, Berlin, Germany

Correspondence
Natalia Cano Murillo, BAM Berlin, Unter den Eichen 87, Berlin 12205, Germany.
Email: natalia.murillo@bam.de

Funding information
Deutsche Forschungsgemeinschaft (DFG), Grant/Award Number: 232311024

Abstract

Thermoplastic modified thermosets are of great interest especially due to their improved fracture toughness. Comparable enhancements have been achieved by adding different nanofillers including inorganic particles such as nanosized boehmite. Here, we present a nanomechanical study of two composite systems, the first comprising a polycarbonate (PC) layer in contact with epoxy resin (EP) and the second consisting of a PC layer containing boehmite nanoparticles (BNP) which is also in contact with an EP layer. The interaction between PC and EP monomer is tested by in situ Fourier transformed infrared (FT-IR) analysis, from which a reaction induced phase separation of the PC phase is inferred. Both systems are explored by atomic force microscopy (AFM) force spectroscopy. AFM force-distance curves (FDC) show no alteration of the mechanical properties of EP at the interface to PC. However, when a PC phase loaded with BNP is put in contact with an epoxy system during curing, a considerable mechanical improvement exceeding the rule of mixture was detected. The trend of BNP to agglomerate preferentially around EP dominated regions and the stiffening effect of BNP on EP shown by spatial resolved measurements of Young's modulus, suggest the effective presence of BNP within the EP phase.

KEYWORDS

composites, mechanical properties, nanoparticles, nanowires and nanocrystals, thermoplastics, thermosets

1 | INTRODUCTION

Epoxies (EP) are widely used thermosetting materials, given their desirable properties such as high-tensile strength and tensile modulus, good chemical resistance and thermal stability. However, their inherent brittleness and low-fracture toughness represent a drawback in industrial applications.[1] For highly cross-linked EP, the addition of a thermoplastic phase, such as polycarbonate (PC), has been proven to overcome some of the shortcomings in mechanical properties.[2] It has been shown also that PC is able to form hydrogen bonds with the

epoxy resin.[3,4] Thus, chemical compatibility is expected between these two phases.

So far, several ways of interaction between PC and EP resins have been documented, such as cross-linking, grafting, or even copolymerization, as well as the possible formation of a semi-interpenetrating polymer network between PC and EP. The latter may occur even in the absence of a curing agent, being triggered mainly by temperature and concentration of PC in the epoxy monomer resin.[5–7]

Besides the combination of EP with PC, other additives like nanosized fillers have been used to improve mechanical properties of the neat resin such as strength, stiffness, and modulus.[8,9] Recently, promising results were achieved by the addition of boehmite (-AlOOH) nanoparticles (BNP). Most remarkably, the increase of shear strength, shear modulus, and compressive strength, as well as an improvement of the fracture toughness of EP by the addition of boehmite were reported.[10,11] The role of BNP as a reinforcement agent was attributed to property alteration of the bulk EP matrix in their presence, and to the formation of a soft interphase, preventing crack propagation by increased energy dissipation.[12] It was demonstrated [13] for an anhydride-cured EP-BNP composite system, that the hardener molecules were preferentially absorbed by the BNP, resulting in the local alteration of the resin-hardener ratio in the bulk. This heterogeneity in the bulk EP, with a broad stiffness distribution, is another pathway for energy dissipation, which makes the system more resistant to fracture.

Based on these improvements, our goal is to develop a new ternary EP composite, consisting of both PC and BNP. Here, BNP acts as a local reinforcement agent, while PC serves as the carrier medium for BNP. This serves to two purposes. First, to decrease the occupational hazards that represent the addition of nanoparticles by, for example, spraying them on specific sites where extra-reinforcement is needed. Second, to optimize BNP distribution throughout the matrix, using a "carrier" material placed as a ply before the resin injection process. However, previous studies demonstrated that, due to the complex interactions between the components of the composite, the overall behavior can drastically deviate from the predictions based on classical theoretical models, such as that of Halpin-Tsai.[14] The effect of BNP on mechanical properties of anhydride-cured EP was reported to drastically differ from the theoretical predictions of composite's modulus. It was found to be mainly due to effects at the nanoscale, such as the formation of mechanical and chemical gradients[15] and soft interphases,[10] migration of the particles to the matrix and the preferential absorption of hardener molecules toward the surface of nanoparticles.[16,17] These are desired effects, since properties of the composite are improved. The subject of this study is to examine the ternary system for comparable effects.

For this purpose, the first step toward understanding a multicomponent composite (PC/BNP/EP) is to study nano effects occurring at the multiple interfaces. This study focuses on interactions between PC/EP and PC/BNP/EP. Interfaces had to be made accessible to the analytical toolset,[18] which can probe molecular and nanomechanical properties, such as atomic force microscopy (AFM). The usage of nanomechanical mapping (e.g., force volume mode) on reactive and nonreactive polymer blends have demonstrated to be reliable for the characterization of the interfacial morphology, width, and mechanical property of the polymer–polymer interphase, making the latter easily evaluated based on the Young's modulus maps with several hundreds of nanometers scan size.[19]

Such studies have also shown the great influence that the polymer interphase can play in the overall mechanical properties. Jiang, Z. et al. proved recently, by PeakForce quantitative nanomechanical mapping (AFM PF-QNM) measurements, how the processing conditions of an immiscible PEEK/PBI blend affect the Young's modulus across the interphase and ultimately the fracture toughness of the blend.[20] The same technique has also proven to be successful for the detection of an enhanced interphase modulus in poly vinyl alcohol/nanodiameter.[21]

We developed two systems, sandwiching a PC layer between two EP layers (Figure 2). One sample contains a neat PC (system A), the second one contains PC filled with BNP (system B). A cross-section of these sandwiched samples provides easy access to the interface, which can then be analyzed by AFM. To probe the nanomechanical properties of interest different techniques were combined. We applied Fourier-transform infrared spectroscopy (FT-IR) to monitor the chemical interaction between DGEBA monomer and PC. Transmission scanning microscopy (T-SEM) was used to study the spatial distribution of the nanoparticles within the composite. The local mechanical properties of the composite phases were measured by AFM force-distance curves (AFM FDC) combined with scanning Kelvin probe microscopy (SKPM).

2 | MATERIALS AND METHODS

2.1 | Materials

The EP system used in this study is bisphenol-A-diglycidyl ether (DGEBA, Araldite LY 556, Huntsman) cured with an anhydride curing agent, methyl

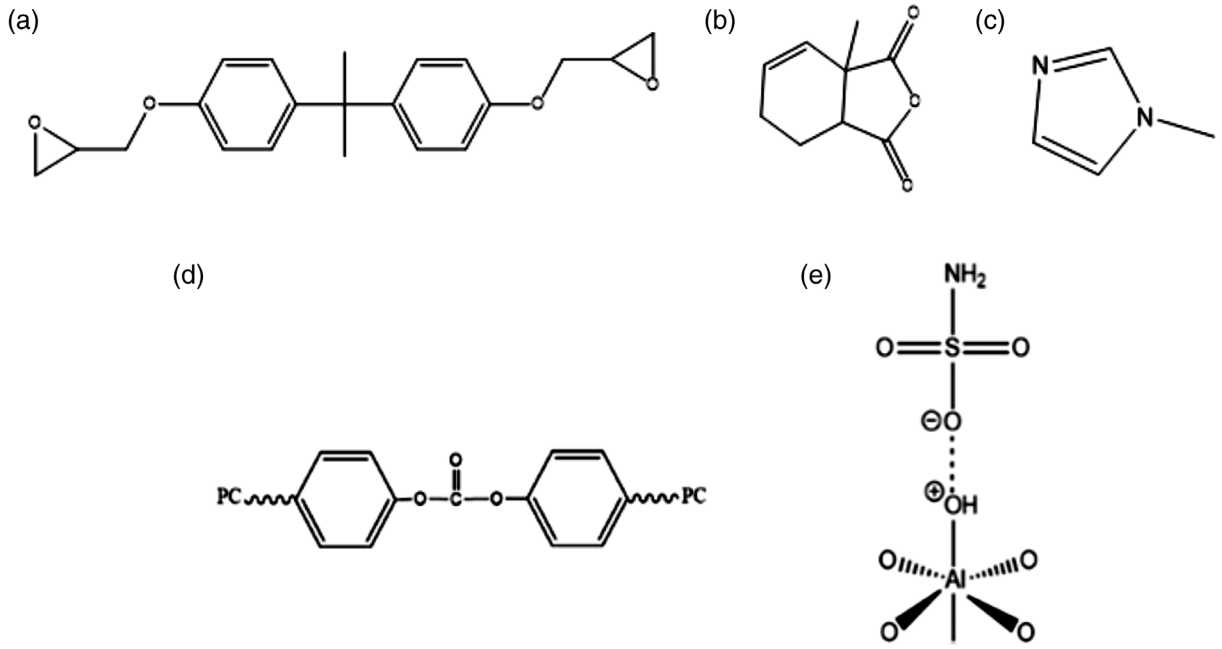

FIGURE 1 Molecular structure of (a) DGEBA epoxy resin. (b) Anhydride hardener MTHPA. (c) Imidazole accelerator. (d) Polycarbonate. (e) Taurine modified boehmite

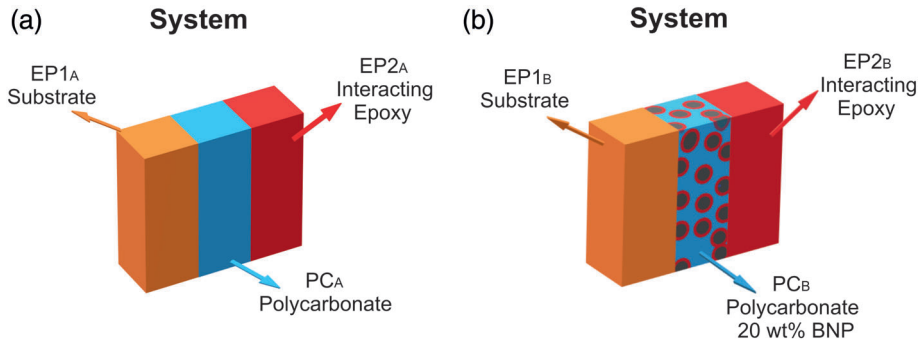

FIGURE 2 Schematic representation of the two systems of interphases between epoxy and polycarbonate (system a) and epoxy and polycarbonate with 20 wt% of BNP (system B). BNP, boehmite nanoparticles; EP, epoxy resin; PC, polycarbonate [Color figure can be viewed at wileyonlinelibrary.com]

tetrahydrophtalic acid anhydride (MTHPA, Aradur HY917, Huntsman) and accelerated by an amine, 1-methyl-imidazole (DY070, Huntsman). The mixture of epoxy, hardener, and accelerator is 100:90:1 parts per weight, respectively. Mixtures are cured for 4 h at 80°C to reach gelation and 4 h at 120°C for post-curing, as recommended by the manufacturer to obtain a fully cured system.[22] The PC is a Bisphenol-A PC from Makrolon 3108 (Goodfellow, UK) with Mw ≈ 49,550 g/mol and Mn ≈ 21,400 as measured by gel permeation chromatography (GPC). BNP are aluminum oxide hydroxide (-AlOOH) boehmite nanoparticles (BNP) (HP14T) with an average primary size of 20 nm, and surface coverage modifications of 1.44 x 10^{-6} mol/m^2. Surface coverage was determined by Brunauer–Emmett–Tellerspecific surface measurements, showing about 16% of the particle surface as taurine modified.[23] The nanoparticles were customized by SASOL Germany. The molecular structures of the used materials are shown in Figure 1.

2.2 | Sample systems for AFM study

System A comprises a substrate of fully cured epoxy substrate ($EP1_A$) and a solution cast film of neat polycarbonate (PC_A) with a concentration of 7 wt% PC in methylene chloride. System B comprises the same fully cured epoxy substrate ($EP1_B$) and a solution cast film of PC from methylene chloride containing 20 wt% of BNP (PC_B) as depicted in Figure 2. The solutions of PC and PC with BNP were dried overnight at room temperature on their EP substrates resulting in a film thickness of 109–128 μm or PC_A and 77–87 μm for PC_B, respectively. Subsequently, in both systems a layer of EP containing the hardener

and the accelerator ($EP2_A$ and $EP2_B$) was poured on top, creating a sandwich-like sample. Before the curing process, the epoxy mixture was left for 45 h at room temperature. Afterwards, the curing process was performed at 80°C for 4 h, followed by post-curing at 120°C for 4 h.

2.3 | Methods

The chemical reactions between epoxy resin (DGEBA) and PC were monitored in situ by FT-IR. These measurements were performed with a Nicolet 8700 FT-IR spectrometer (Thermo Electron Corporation, Madison, WI) in transmission mode. The heating stage, a Linkam FT-IR 600, was placed in the spectrometer and controlled by a TMS94 temperature controller. FT-IR measurements were performed within a wavelength range from 400 to 4000 cm^{-1} and with a resolution of 4 cm^{-1}, by averaging eight scans. For the sample preparation, PC and DGEBA were mixed in a 1:1 ratio in methylene chloride CH_2Cl_2 and stirred overnight. The solution was spin-coated on pressed KBr pellets and mounted inside the heating cell in transmission mode. The PC/DGEBA film was heated within the spectrometer to 80°C for 60 min, followed by a second heating at 120°C for another 60 min. The spectra were recorded with a time interval of 30 s per spectrum by the OMNIC software (Thermo Fisher Scientific, Karlsruhe, Germany). Except for the background subtraction no additional data treatment was applied. None of the IR spectra showed one of the typical absorption bands of the solvent CH_2Cl_2.

All AFM measurements were conducted with an MFP-3D AFM (Asylum Research, Santa Barbara, CA). The AFM probe used was a Mikromasch, HQ: NSC35 (Wetzlar, Germany). The spring constant of the cantilever was determined by a noninvasive thermal noise method to be $k_c = 14.2$ N/m. The tip radius $R = 23$ nm was estimated by fitting reference measurements on glass substrates ($E = 70$ GPa, vs $= 0.3$) with the Hertz theory (compare Supplementary information Equation (S4)). FDC were recorded with a frequency of 1 Hz and 1 μm apart from each other, leading to 60 x 60 curves for a sample area of 60 x 60 μm^2, leading to one data point (pixel) per 1 μm in all FDC maps. Maximum applied force was 0.7 μN. The detailed methodology of analyzing FDC curves is described in reference [24]. In a subsequent step, each curve was analyzed and fitted by the Hertz theory yielding spatially resolved Young's Modulus maps. For the analysis of FDC, we used a custom software developed in our group. For a statistical analysis, histograms of the Young's Modulus maps were plotted. To separate contributions of the different material phases, and their possible interphases, these histograms were analyzed further. Therefore, they were deconvoluted into multiple Gaussians (Fityk software[25]), which were assigned to the different phases. SKPM was used to probe the surface potential to visualize material contrast independent of the mechanics of the surface. The maps of the surface potential are used to determine and locate BNP and their aggregates. The information about the location of BNP is then included in the analysis of FDC maps of the corresponding area. In the SKPM method, an AFM tip is brought close to the sample surface and their electrostatic interaction can be described by a capacitor plate model. Surface potential difference is generated between the tip and sample surface due to the differences in their Fermi energy levels. An AC voltage is applied to the tip corresponding to the resonance frequency of the cantilever. The resulting surface potential difference between the tip and the sample induces mechanical oscillations in the cantilever. By applying an additional DC voltage to the cantilever, this mechanical oscillation is canceled out. The voltage required to nullify the mechanical oscillation corresponds to the surface potential of the sample. The corresponding equations and technical considerations are described in detail elsewhere.[26]

The spatial distribution of BNP in system B was investigated by scanning electron microscopy (SEM) using a Zeiss Supra 40 microscope (Zeiss, Oberkochen, Germany) equipped with a high-resolution cathode of Schottky type and conventional Everhart-Thornley (ET) and In-lens secondary electron (SE) detectors. For better observation of the nanoparticles in the sample volume, the SEM was operated in the transmission mode, that is, the so-called T-SEM mode.[27] For this purpose, free-standing 100 nm thin sections of the samples PC-EP and PC-BNP-EP were prepared by ultramicrotomy and deposited on a typical copper TEM grid.

3 | RESULTS AND DISCUSSION

3.1 | System A: Morphology of the interphases

Figure 3 middle shows the morphology of system A under an optical microscope. The AFM tapping mode topography of the interfacial region between $EP1_A$ and PC_A is shown in Figure 3 left. The interfacial boundary is clearly defined. This is because $EP1_A$ was already cured before PC_A was brought into contact and thus, formation of an interphase with mixed properties is not expected.

The topography image of the interfacial region between PC_A and $EP2_A$ (Figure 3, right) is significantly different from that between $EP1_A$ and PC_A (Figure 3, left). The topographical features of PC_A are spherulite-

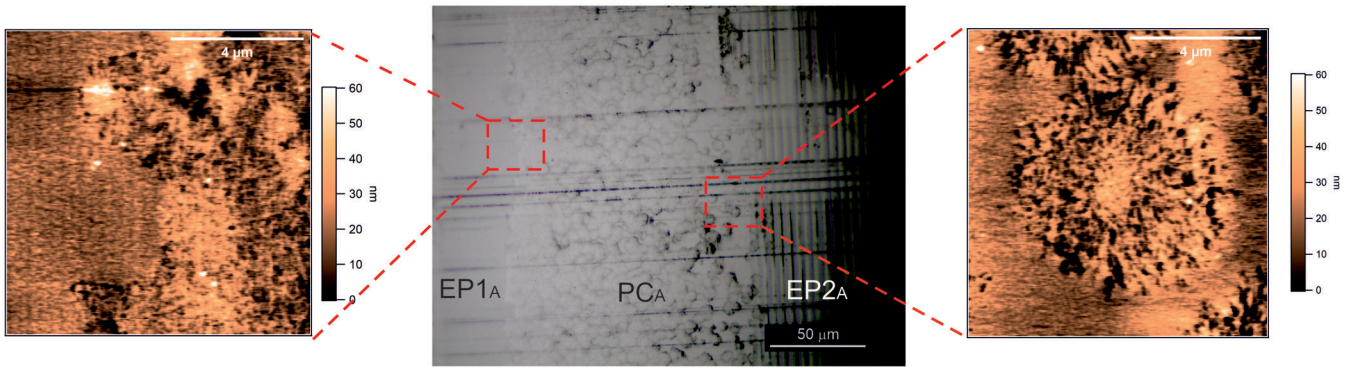

FIGURE 3 Left: AFM tapping mode topography (height) of the interfacial region between $EP1_A$ and PC_A. Middle: Optical micrograph of the cross-section of the system. Right: Topography (height) of the interfacial region between PC_A and $EP2_A$. AFM, atomic force microscopy; EP, epoxy resin; PC, polycarbonate [Color figure can be viewed at wileyonlinelibrary.com]

like and are perfectly distinguishable from EP. Although PC is inherently an amorphous thermoplastic material, it can crystallize under specific circumstances, as Siegmann et al. found, using CH_2Cl_2 as a solvent.[28,29] Accordingly, a PC film cast from CH_2Cl_2 solution will form spherulites when annealed between 80°C and its glass transition temperature (T_g) of 149°C. In our case, the applied curing conditions are matching the required temperature, and consequently, crystallization of PC_A occurs (Figure 3, right). In addition, the formation of spherulites is also promoted by the interaction between PC and the secondary hydroxyl groups of the DGEBA. Liang et al.,[30] showed that DGEBA acts as a plasticizer for PC and increases its chain mobility, causing a reduction of T_g of PC and thus an increase in its crystallization rate. Moreover, the concentration of PC in contact with the DGEBA resin influences possible interactions. At low concentrations of PC, the availability of secondary hydroxyl groups from DGEBA is higher, which leads to an increased interaction probability with the carbonyl group in PC. This behavior can be mainly associated with the H-bonding and/or trans-ester reactions.[2] Using our mentioned ternary composition eventually for technical purposes, it would be interesting to know if both polymer components used in this work behave similarly.

3.2 | In situ monitoring of the PC and epoxy interaction by FT-IR

To provide evidence whether the PC-DGEBA interaction is associated with H-bonding and/or trans-ester reactions as mentioned above, FT-IR measurements were performed resembling the curing conditions. Figure 4(a) shows IR absorption in the region of carbonyl group stretching mode. During the first heating stage at 80°C a broad bimodal peak was measured with maxima at 1776

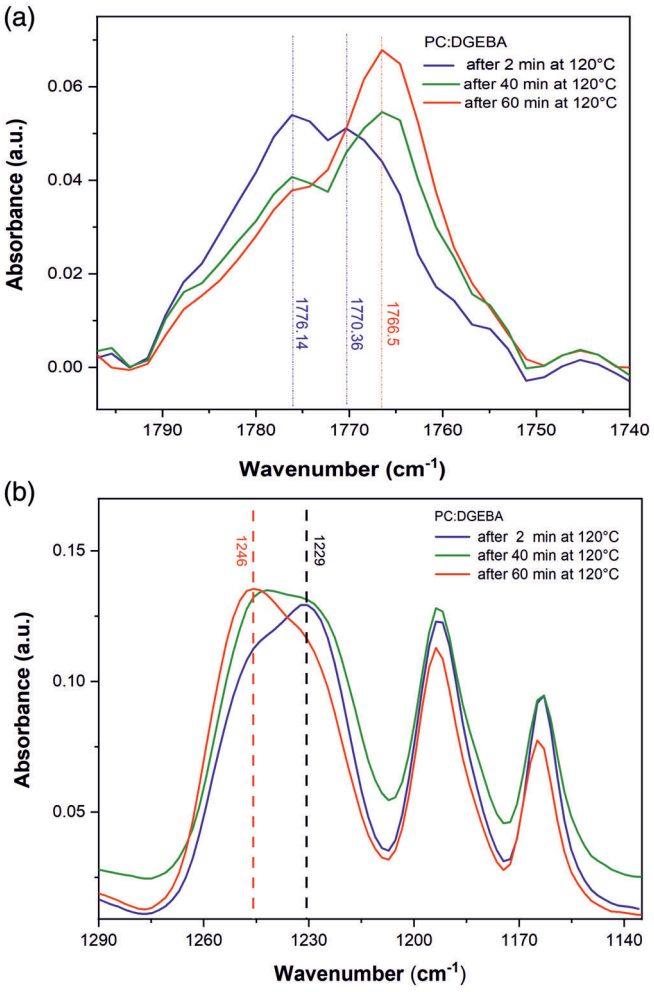

FIGURE 4 FT-IR spectra of the sample at the beginning of the two-step curing process (blue curves), after 40 min at 120°C (green curves) and 60 min at 120°C (red curves) of heating. (a) Carbonyl region from 1776 to 1766 cm^{-1} in a mixture of PC and DGEBA 1:1 (b) Changes in region of O—C—O stretching of the same DGEBA/PC mixture during heating up to 120°C. FT-IR, Fourier transformed infrared; PC, polycarbonate [Color figure can be viewed at wileyonlinelibrary.com]

and 1770 cm^{-1}, which corresponds to the absorption of carbonate, linked C═O group. After 40 min at 120°C, the two peaks diminish in intensity and a better-defined peak at 1766 cm^{-1} becomes predominant, while a small shoulder of the 1776 cm^{-1} is still present (Figure 4(a), green curve). The aliphatic linkage of the C═O absorbing at 1766 cm^{-1} becomes even more intense after 60 min of heating at 120°C (Figure 4(a), red curve).

Additional changes were observed in the region of O—C—O stretching (Figure 4(b)). The observed increase of the 1246 cm^{-1} peak compared to the 1229 cm^{-1} is related to exchange reactions like esterification. The latter implies a bonding of hydrolyzed chains of PC, which are able to form linkages with the epoxy chain.[31] Hence, this observation indicates that PC/DGEBA system interacts in a way that PC is likely to be incorporated later into the epoxy chain.

In a system like PC/DGEBA, the behavior can be expected to be similar to that of a thermoplastic modified thermoset resin, since a reaction induced phase separation was already described. From the results of IR spectroscopy, the phases are compatible and do interact. During curing of EP, its molar mass increases and phase separation from PC occurs.[32] Thus, the energy of mixing is changed and spinodal decomposition, as well as nucleation and growth of the thermoplastic phase, are energetically favored.[33] At the end of the phase separation, both phenomena lead to separated spherical domains of a thermoplastic-rich phase. Therefore, it was concluded that all these phenomena result from the interdiffusion of phases.

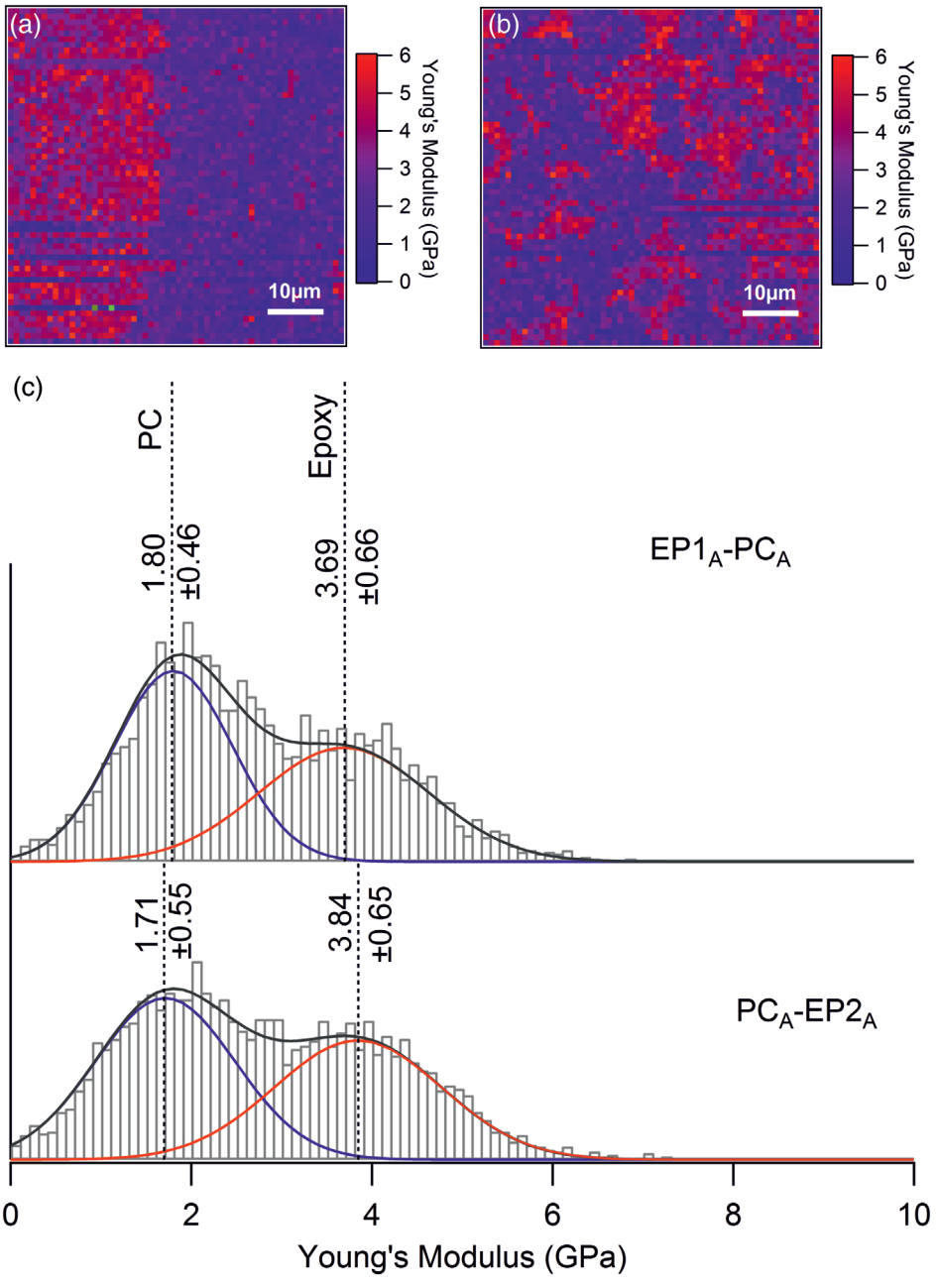

FIGURE 5 Young's modulus map of (a) $EP1_A$-PC_A and (b) PC_A-$EP2_A$ interfacial regions of system A. (c) Comparison of the Young's moduli histogram and their deconvolution by Gaussian fit (red and blue curves correspond to EP and PC, respectively). EP, epoxy resin; PC, polycarbonate [Color figure can be viewed at wileyonlinelibrary.com]

3.3 | System A: Nanomechanical properties of the interphases

FDC curves were obtained at the interfacial region on both sides of the composite, thereby providing information about the mechanical properties of the neat materials ($EP1_A$ and PC_A) and the binary composite (PC_A-$EP2_A$) with high lateral resolution. As mentioned above, each FDC was fitted by the Hertz model, yielding the Young's Modulus for each measuring point.[34] Figure 5 shows the Young's Modulus maps corresponding to the interfacial areas of $EP1_A$-PC_A (Figure 5(a)) and of PC_A-$EP2_A$ (Figure 5(b)). The two material phases can be clearly distinguished, showing that the Young's Modulus of PC_A (blue region) is noticeably lower than the one of $EP1_A$ and $EP2_A$ (red region).

For quantitative evaluation and comparison of the mechanical properties histograms of the Young's Modulus were extracted (Figure 5(c)). In the case of ($EP1_A$-PC_A) no interaction between the components is expected. Thus, the observed distribution of the Young's Modulus is assigned to the characteristics of the neat materials. Then, Gaussian deconvolution allows to separate the contributions of the pure PC phase and the pure EP phase in the noninteracting $EP1_A$ region. In case of the binary composite (PC_A-$EP2_A$), an interaction of the material phases was established by FT-IR measurements (compare Section 3.2). The question remains, if this influences the mechanical properties of the composite: either by forming an interphase (a third phase with distinguishable properties) or by affecting the bulk directly (changing the properties of one or both phases significantly). From the comparison of both deconvoluted histograms, we conclude that neither a third component is appearing, nor the average Young's Modulus of both phases changes significantly. Basically the histograms of $EP1_A$-PC_A and PC_A-$EP2_A$ are identical and show the same average Young's Modulus which corresponds to the neat materials ($E_{PC} = 1.7 \pm 0.55$ GPa and $E_{EP} = 3.8 \pm 0.65$ GPa). Thus, we conclude that, despite an observable chemical interaction between PC and DGEBA, the exposure of PC in EP has no observable influence on the mechanical properties, when compared to the neat materials.

3.4 | System B: Spatial distribution and nanomechanical study on the interphases

The spatial distribution of BNP in system B was studied by T-SEM measurements, performed on approx. 100 nm thick, ultra-microtomed slices of system B cross-sections. It should be noticed here, that the T-SEM transmission mode is rather sensitive to changes in the atomic number in the bulk of the electron transparent constituent material, and that this superior material contrast is visible with a spatial resolution of only a few nm. The three phases are very well distinguishable as shown in Figure 6. Here, EP is showing a lighter gray level as compared to PC and BNP, which are represented by a darker gray level. The PC phase in System B appears to be more homogeneous, and no spherulite-like structures were detected. A well-defined border between $EP1_B$ and PC_B is evident. The interacting PC_B-$EP2_B$ region shows a blurry, less well-defined border. This can be the consequence of a partial dissolution of PC in $EP2_B$, resulting in PC

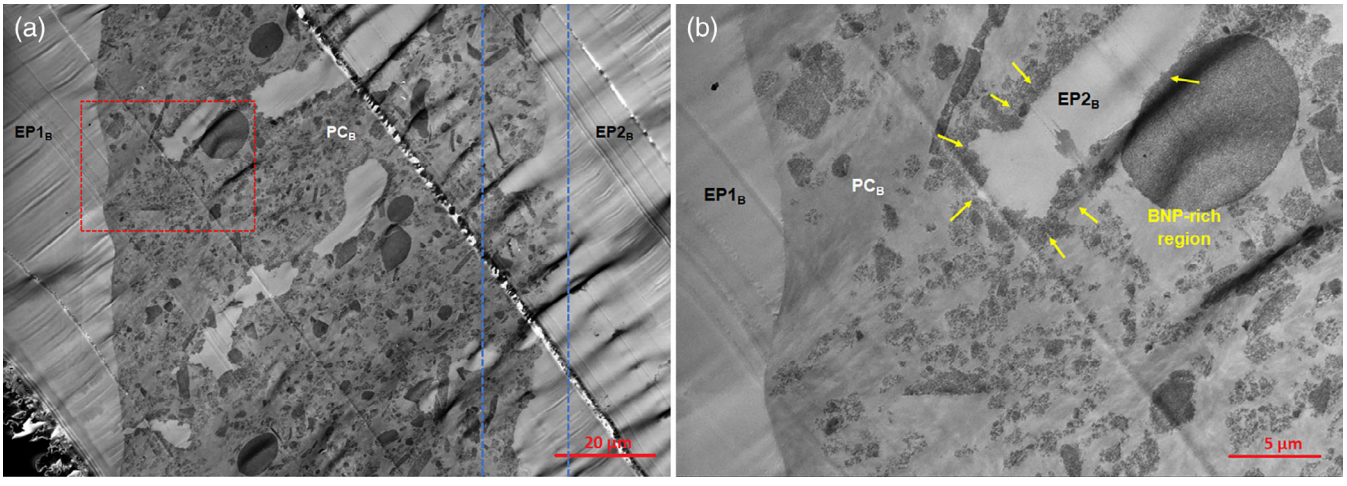

FIGURE 6 (a) Scanning electron micrograph in the transmission mode (T-SEM) of system B prepared as ultra-microtomed slice (~100 nm thickness) in cross-section. The interfacial region of interest (PC_B -$EP2_B$) is located in between the blue lines. The dashed square corresponds to the zoomed-in area in b. (b) the zoomed-in area in which BNP agglomerate around the EP inclusion (see yellow arrows). BNP, boehmite nanoparticles; EP, epoxy resin; PC, polycarbonate [Color figure can be viewed at wileyonlinelibrary.com]

regions with decreased density. In some regions, $EP2_B$ is even penetrated and trapped in PC, which is another indication of interaction between $EP2_B$ and PC_B phases. The high concentration (20 wt%) of BNP in PC resulted in the formation of large, tight agglomerates, visible as dark small spots in the PC_B.

It is noteworthy that there are regions in which BNP are agglomerated around the EP phase (see Figure 6(b)). This might be due to the competing processes of self-aggregation of BNP inside the PC, and the preferential migration of BNP toward $EP2_B$. In the latter case, it is anticipated that local mechanical properties of epoxy are influenced by the presence of BNP.[17] This hypothesis is further verified by comparison of the nanomechanical properties of PC_B and $EP2_B$ with those of system A.

Figure 7(a) shows the topography, of a representative area within the PC_B-$EP2_B$ interfacial region (as marked with blue lines in Figure 6(a)) obtained by AFM. From the topography map, the PC and EP phases are distinguishable, since the cross-sectional cut on PC region generates a rougher surface as compared to that of EP. However, identifying BNP solely based on topographic features is a challenging task. It has been demonstrated by Ghasem Zadeh Khorasani et al.[12] on similar composites that during SKPM measurements, BNP appear with a higher surface potential than epoxy. Here, we also apply SKPM to locate the BNP (brighter spots in Figure 7(b)) in the epoxy matrix. These AFM scans, together with the T-SEM micrograph, allow us to distinguish between the three regions, which are dominated by

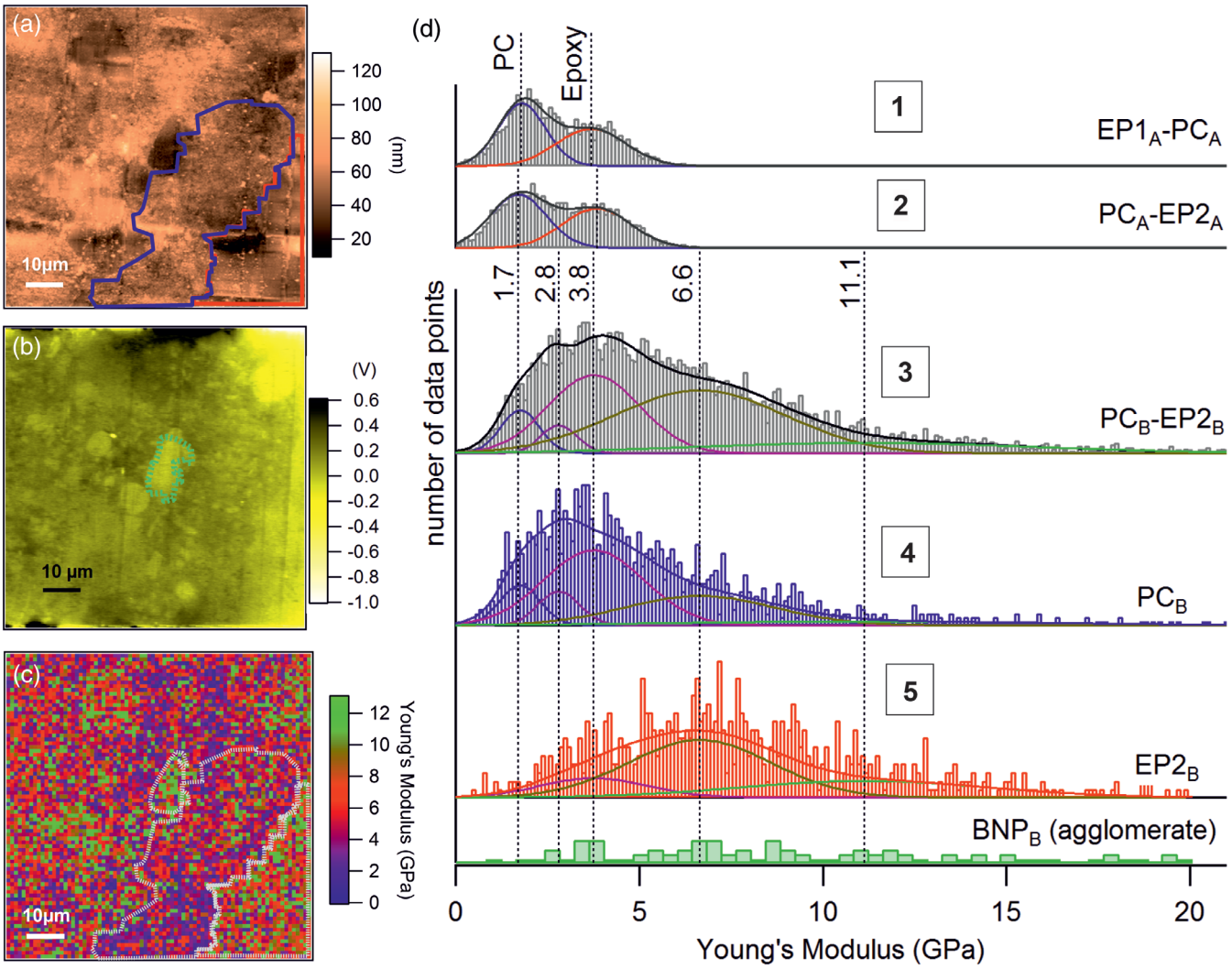

FIGURE 7 (a) AFM tapping mode topography of a selected area (80 x 80 μm^2) in the interfacial region between PC_B-$EP2_B$ with a marked PC-BNP region (blue) and an $EP2_B$ area (red) (b) SKPM map of the same selected area as (a) with a marked bright BNP-rich region within PC_B (green) (c) Young's modulus map of a selected area (same as (a)) in the interface region PC_B-$EP2_B$ and (d) histograms of the corresponding Young's modulus maps. For details, see the text. AFM, atomic force microscopy; BNP, boehmite nanoparticles; EP, epoxy resin; PC, polycarbonate; SKPM, scanning Kelvin probe microscopy [Color figure can be viewed at wileyonlinelibrary.com]

TABLE 1 Young's modulus E calculated from the fitting of the histograms 1–2 shown in Figure 7(d) and calculated as described in Supporting Information 1.

System A	Histogram		E_{PC}	E_{epoxy}
	1	$EP1_A$-PC_A	1.80 ± 0.46	3.69 ± 0.66
	2	PC_A-$EP2_A$	1.71 ± 0.55	3.84 ± 0.65

Abbreviations: EP, epoxy resin; PC, polycarbonate.

either PC (Figure 7(a) blue line), EP (Figure 7(a) red line) or BNP (Figure 7(b) dotted green line). Since we are mainly interested in the mechanical properties of the sample, an AFM FDC force map was taken from the same region. Comparing the Young's Modulus maps of the binary system A with the ternary system B (Figure 7 (c)) it is observed that the overall mechanical properties changed dramatically, since the overall Young's Modulus of system B increased up to a factor of two. To understand the origin of this change in mechanical properties, we had a closer look at the distribution of Young's Modulus (Figure 7(d)). For comparison, the histograms of the binary systems are included in the graph, and the Young's Modulus of all regions are summarized in Table 1 and Table 2. The characteristic values for $E_{PC} = 1.7 \pm 0.55$ and $E_{EP} = 3.8 \pm 0.65$ GPa were kept as fixed values for all subsequent deconvolutions.

The histogram of the ternary system B (Figure 7(d), third histogram), comprised of PC_B, BNP, $EP2_B$, is very different and shows an extension to stiffer values. For a deconvolution of the histogram, three additional Gaussians were added. They represent the intermediate behavior between PC and EP (mixed moduli, 2.8 and 6.6 GPa) and the influence of the BNP (11.1 GPa), respectively. In order to understand the contribution from the different materials to this overall mechanical behavior, histograms of Young's Modulus values are displayed for comparison. They correspond to PC dominated (dashed blue line) EP dominated (dashed red line) and BNP dominated (dashed green line) regions. When deconvoluting these histograms, the acquired center value (x_0) of the respective Gaussian from the fit before was kept as fixed fit parameters. The distribution of BNP and the central value of around 11.1 GPa is in agreement with the typical Young's Modulus value of boehmite, as measured by Fankhänel et al.[24] For the PC dominated region, the deconvolution shows contributions from neat PC, but most points result in a stiffness similar to that of the bulk EP. This could be due to the inclusion of epoxy into the PC dominated region or stiffening of PC by the BNP. Interestingly, an intermediate behavior (fit with $x_0 = 2.8$ GPa) is also observed. This indicates a gradual stiffening effect, and not a bimodal distribution. This might be an additional indication for a stiffening of PC by the BNP. On the other hand, there are also values found well above 3.8 GPa, which are typical for stiffened epoxy and could indicate the presence of epoxy in the PC dominated area. The stiffened epoxy can be seen in the histogram of the epoxy dominated region $EP2_B$, with a clear maximum around 6.6 GPa. This agrees with previous results, according to which BNP stiffens the epoxy matrix by disrupting the reaction between anhydride hardener with the epoxy monomer.[17] Moreover, some regions in the histogram of $EP2_B$ showed even higher values, corresponding to the typical Young's Modulus value of BNP. This being an indication of the presence of BNP in the $EP2_B$ dominated region. From this, we hypothesize that the contact region between PC and EP is a region in which BNP can migrate and affect the molecular architecture of the cross-linked EP, causing a reinforcing effect. Given the increased chain mobility of the PC phase, and that the interaction between PC and EP is proven, it is possible to use this compatibility between the phases to carry nanoparticles into an epoxy system and achieve a stronger local reinforcement effect.

In general, it is beneficial for the overall mechanical performance of a composite, to have homogeneous distribution of the nanofiller, since bigger agglomerates (>5 μm) are often associated with mechanical singularities in nano composites. However, we would like to point out here, that this is not the case for the system presented. By looking at the mechanical properties of such agglomerates (Figure 7(b), green dotted line) it is obvious that the agglomerates show a broad distribution of mechanical properties, which matches the properties of the overall system B. Therefore, we conclude that although the T-SEM image shows an inhomogeneous

TABLE 2 Young's modulus E calculated from the fitting of the histograms 3–5 shown in Figure 7(d) and calculated as described in Supporting Information 1.

System B	Histogram		E_{PC}	$E_{PC,stiffened}$	$E_{PC,stiffened}$	E_{epoxy}	$E_{epoxy,stiffened}$	$E_{boehmite}$
	3	PC_B-$EP2_B$	1.76 ± 0.38	2.80 ± 0.35		3.77 ± 0.39	6.6 ± 1.64	11.1 ± 3.34
	4	PC_B dominated	1.76 ± 0.40*	2.80 ± 0.41*	3.77 ± 0.96*		6.6 ± 1.45*	
	5	$EP2_B$ dominated				3.77 ± 1.03*	6.6 ± 1.37*	11.1 ± 2.39*

Abbreviations: EP, epoxy resin; PC, polycarbonate.

*Values that are kept as fixed parameters.

phase distribution at the nanometer scale, this inhomogeneity is not reflected in the mechanical properties, as can be seen in the histogram (Figure 7(d)).

4 | CONCLUSIONS

We successfully assessed the nanomechanical properties of the epoxy (EP) PC composites, with and without the presence of BNP, on the micro scale, by studying the cross-section of a layered composite systems. This approach enabled us to study the interphase between EP and PC and its changed properties upon addition of the BNP. An interaction between the PC and the EP phases was observed by FT-IR in situ monitoring. Such interaction comprised the aliphatic linkage from some PC chains to the epoxy monomer. An ultimately phase separation of the PC from the EP was detectable by AFM-FDC mapping. As expected from the phase separation, the two phases behaved mechanically independently without any gradient of the nanomechanical properties and the Young's Modulus of the PC as well as that of the EP phase remained unaltered.

In the case of the ternary system, the three phases were distinguishable as shown by T-SEM and SKPM. This allowed us to discriminate areas between the components and to make their interphases accessible for AFM-FDC analysis. A deconvolution of the histograms of the Young's Modulus accounts for the detection of several phase contributions in the scanned area. A PC dominated region appear to be stiffened by the BNP, showing intermediate stiffness values in comparison to those corresponding to the neat PC and neat EP. Even higher stiffness values, compared to those of the neat EP were registered, which suggests the presence of stiffened EP inside this PC dominated region. In the case of the interacting EP region, the trend toward higher stiffness values remained and the Young's Modulus increased up to a factor of two for the overall scanned area. This remarkable effect was already shown to be due to the presence of nanoparticles within the epoxy phase, enhancing the mechanical properties beyond the rule of mixture. Further studies will focus on exploring the effects of composite BNP-PC fibers embedded in an epoxy matrix, and their potential to enhance stiffness in specific regions of fiber-reinforced composites.

ACKNOWLEDGMENTS

The work was funded by the Deutsche Forschungsgemeinschaft (DFG) in the frame of a research unit FOR2021: "Acting principles of nano-scaled matrix additives for composite structures" with project number 232311024 and Colciencias Scholarship number 679. Furthermore, the authors gratefully acknowledge Tassilo Waniek for assisting with the FT-IR measurements, Mrs. Sigrid Benemann for technical assistance at the SEM measurements and Mrs. Liliana Gonzalez for the structural drawings.

ORCID

Natalia Cano Murillo https://orcid.org/0000-0003-1362-611X
Dorothee Silbernagl https://orcid.org/0000-0001-8572-3184
Marc Benjamin Hahn https://orcid.org/0000-0002-5050-7083

REFERENCES

[1] K. P. Unnikrishnan, E. T. Thachil, *Des. Monomers Polym.* **2006**, *9*, 129.
[2] T.-M. Don, J. P. Bell, *J. Polym. Sci. A Polym. Chem.* **1996**, *34*, 2103.
[3] E. M. Woo, C. C. Su, *Polym. J.* **1997**, *29*, 514.
[4] E. M. Woo, M. N. Wu, *Polymer* **1996**, *37*, 2485.
[5] M. Rong, H. Zeng, *Polymer* **1996**, *37*, 2525.
[6] M. Rong, H. Zeng, *Polymer* **1997**, *38*, 269.
[7] M.-S. Lin, S.-T. Lee, *Polymer* **1997**, *38*, 53.
[8] J. Njuguna, K. Pielichowski, *Adv. Eng. Mater.* **2003**, *5*, 769.
[9] S. Sprenger, *J. Appl. Polym. Sci.* **2013**, *130*, 1421.
[10] M. Jux, J. Fankhänel, B. Daum, T. Mahrholz, M. Sinapius, R. Rolfes, *Polymer* **2018**, *141*, 34.
[11] M. Jux, B. Finke, T. Mahrholz, M. Sinapius, A. Kwade, C. Schilde, *J. Nanopart. Res.* **2017**, *19*, 241.
[12] M. Ghasem Zadeh Khorasani, D. Silbernagl, D. Platz, H. Sturm, *Polymers* **2019**, *11*, 235.
[13] M. Ghasem Zadeh Khorasani, A.-M. Elert, V.-D. Hodoroaba, L. Agudo Jácome, K. Altmann, D. Silbernagl, H. Sturm, *Nanomaterials (Basel, Switzerland)* **2019**, *9*, 853.
[14] Y. Zare, *Polym. Test.* **2016**, *51*, 69.
[15] M. Munz, H. Sturm, W. Stark, *Polymer* **2005**, *46*, 9097.
[16] K. Caldwell, J. C. Berg, *J. Compos. Mater.* **2017**, *51*, 3877.
[17] M. Ghasem Zadeh Khorasani, D. Silbernagl, P. Szymoniak, V.-D. Hodoroaba, H. Sturm, *Polymer* **2019**, *164*, 174.
[18] J. Chung, M. Munz, H. Sturm, *Surf. Interface Anal.* **2007**, *39*, 624.
[19] D. Wang, S. Fujinami, H. Liu, K. Nakajima, T. Nishi, *Macromolecules* **2010**, *43*, 5521.
[20] Z. Jiang, P. Liu, Q. Chen, H.-J. Sue, T. Bremner, L. P. DiSano, *J. Appl. Polym. Sci.* **2020**, *137*, 48966.
[21] M. Mousa, Y. Dong, *Nanotechnology* **2018**, *29*, 385701.
[22] Huntsmann Advanced Materials. Araldite LY 556/Aradur HY 906/Accelerator DY 070: Datasheet; **2012**. Available online: https://apps.huntsmanservice.com/WebFolder/ui/browse.do?pFileName=/opt/TDS/Huntsman%20Advanced%20Materials/English/Long/Araldite%20LY%20556_Aradur%20906_Accelerator%20DY070_eur_e.pdf.
[23] W. Exner, C. Arlt, T. Mahrholz, U. Riedel, M. Sinapius, *Compos. Sci. Technol.* **2012**, *72*, 1153.
[24] J. Fankhänel, D. Silbernagl, M. Ghasem Zadeh Khorasani, B. Daum, A. Kempe, H. Sturm, R. Rolfes, *J. Nanomater.* **2016**, *2016*, 1.
[25] M. Wojdyr, *J. Appl. Cryst.* **2010**, *43*, 1126.

[26] W. Melitz, J. Shen, A. C. Kummel, S. Lee, *Surface Sci. Reports* **2011**, *66*, 1.
[27] V.-D. Hodoroaba, C. Motzkus, T. Macé, S. Vaslin-Reimann, *Microsc. Microanal.: Off. J. Microsc. Soc. Am., Microbeam Anal. Soc., Microsc. Soc. Canada* **2014**, *20*, 602.
[28] A. Siegmann, P. H. Geil, *J. Macromol. Sci., Part B* **1970**, *4*, 239.
[29] A. Siegmann, P. H. Geil, *J. Macromol. Sci., Part B* **1970**, *4*, 273.
[30] G. G. Liang, W. D. Cook, A. Tcharkhtchi, H. Sautereau, *Eur. Polym. J.* **2011**, *47*, 1578.
[31] M.-S. Li, Y.-F. Su, C.-C. M. Ma, J.-L. Chen, M.-S. Lu, F.-C. Chang, *Polymer* **1996**, *37*, 3899.
[32] B. S. Kim, T. Chiba, T. Inoue, *Polymer* **1995**, *36*, 67.
[33] S. Goossens, B. Goderis, G. Groeninckx, *Macromolecules* **2006**, *39*, 2953.
[34] H.-J. Butt, B. Cappella, M. Kappl, *Surface Sci. Reports* **2005**, *59*, 1.

SUPPORTING INFORMATION

Additional supporting information may be found online in the Supporting Information section at the end of this article.

How to cite this article: Cano Murillo N, Ghasem Zadeh Khorasani M, Silbernagl D, Hahn MB, Hodoroaba V-D, Sturm H. Nanomechanical study of polycarbonate/boehmite nanoparticles/epoxy ternary composite and their interphases. *J Appl Polym Sci*. 2020;e50231. https://doi.org/10.1002/app.50231